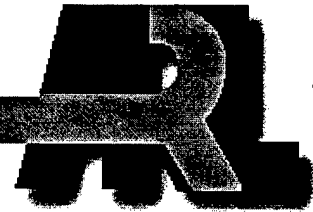


ARMY RESEARCH LABORATORY



Conduction in Electrically Exploded Wires of Nonuniform Diameters

Clinton E. Hollandsworth
John D. Powell
Michael J. Keele
Charles R. Hummer

ARL-TR-1773

DECEMBER 1998

19990114 050

The findings in this report are not to be construed as an official Department of the Army position
unless so designated by other authorized documents.

Citation of manufacturer's or trade names does not constitute an official endorsement or approval of
the use thereof.

Destroy this report when it is no longer needed. Do not return it to the originator.

REPRODUCTION QUALITY NOTICE

This document is the best quality available. The copy furnished to DTIC contained pages that may have the following quality problems:

- **Pages smaller or larger than normal.**
- **Pages with background color or light colored printing.**
- **Pages with small type or poor printing; and or**
- **Pages with continuous tone material or color photographs.**

Due to various output media available these conditions may or may not cause poor legibility in the microfiche or hardcopy output you receive.



If this block is checked, the copy furnished to DTIC contained pages with color printing, that when reproduced in Black and White, may change detail of the original copy.

Army Research Laboratory

Aberdeen Proving Ground, MD 21005-5066

ARL-TR-1773

December 1998

Conduction in Electrically Exploded Wires of Nonuniform Diameters

Clinton E. Hollandsworth
John D. Powell
Michael J. Keele
Charles R. Hummer
Weapons & Materials Research Directorate

Approved for public release; distribution is unlimited.

Abstract

Recent work by Me-Bar and Harel, intended to characterize the conduction characteristics of exploding segmented wires, is extended. A set of experiments on conductors composed of various materials and in various geometries was undertaken. The experimental work is complemented by two-dimensional calculations in which the magnetic diffusion equation is solved for the problems at hand. Results from these calculations are used to explain the behavior observed in the experiments. It is also observed from the calculations that different results for segmented wires might be obtained if the plasma, resulting from partial explosion of the wires, is confined radially around the wire. A set of experiments to test this contention was undertaken and produced results in good qualitative agreement with the theoretical predictions. Physical reasons for the observed behavior, as well as possible methods for ameliorating undesired effects, are indicated.

ACKNOWLEDGMENTS

The authors thank Jad H. Batteh for a number of useful discussions.

DTIC QUALITY ASSURED 3

INTENTIONALLY LEFT BLANK

TABLE OF CONTENTS

	<u>Page</u>
LIST OF FIGURES	vii
LIST OF TABLES	ix
1. INTRODUCTION	1
2. EXPERIMENTAL SETUP	3
3. EXPERIMENTAL RESULTS	4
4. CALCULATIONS	10
5. EFFECTS OF PLASMA CONFINEMENT	14
6. SUMMARY AND CONCLUSIONS	20
REFERENCES	21
APPENDIX A. DIGITIZED RADIOGRAPHS FOR ALL TESTS WITH UNCONFINED WIRES	23
DISTRIBUTION LIST	35
REPORT DOCUMENTATION PAGE	37

INTENTIONALLY LEFT BLANK

LIST OF FIGURES

<u>Figure</u>	<u>Page</u>
1. Experimental setup for Shots S ₁₄ Through S ₂₂	4
2. Dimensions of Samples Employed in Shots S ₁₄ Through S ₂₂	5
3. Radiographic Results for the Explosion of the Segmented Brass Wire in Shot S ₁₅ .	6
4. Radiographic Results Demonstrating Acceleration by the Lorentz Force for the Copper Wire in Shot S ₁₇	7
5. Current I (dotted curve) and Time Derivative dI/dt (solid curve) for Shot S ₁₅	8
6. Resistance Versus Time for Shot S ₁₄ , Corresponding to a Smooth Wire (solid curve), and Shot S ₁₅ , Corresponding to a Segmented Wire (dotted curve)	9
7. Model Employed in Calculations: (a) a Periodic Array of Cylindrically Symmetrical, Solid and Plasma Conductors; (b) the Calculation Domain That Lies Between Lines L ₁ and L ₂ in Part (a).	11
8. Current Streamlines in Calculation Domain for Two Limiting Cases: (a) $\bar{r}_m \gg \bar{z}_m$; (b) $\bar{r}_m \ll \bar{z}_m$	13
9. Experimental Setup for Plasma-Confinement Experiments	15
10. Experimental Results for Test T ₂ : (a) X-ray Images; (b) Photograph of Recovered Segments	16
11. Wire Dimensions and Geometry for Plasma-Confinement Experiments	17
12. Calculated Current Streamlines for the Geometry Employed in the Plasma-Confinement Experiments	18
13. Radiographic Results From Plasma-Confinement Experiments: (a) Test T ₄ (thin walled Lexan sleeve); (b) Test T ₅ (thick walled Lexan sleeve)	19

INTENTIONALLY LEFT BLANK

LIST OF TABLES

<u>Table</u>	<u>Page</u>
1. Data for Shots S_{14} Through S_{22}	5
2. Data for Shots T_1 Through T_5	16

INTENTIONALLY LEFT BLANK

CONDUCTION IN ELECTRICALLY EXPLODED WIRES OF NONUNIFORM DIAMETER

1. INTRODUCTION

Thin wires, a few mils in diameter, are easily exploded by connecting them to a charged capacitor (or, in earlier times, a Leyden jar) of reasonable size. Experimental work with exploding wires was reported in the *Philosophical Transactions of the Royal Society (London)* as early as 1774, according to Chace [1]. It is not surprising that interest has continued in this phenomenon: the event is always accompanied by a loud noise and a brilliant flash of light. Genuine scientific interest, however, was first aroused in the 1920s when Anderson [2] showed that the temperatures produced approached those on the sun. Scientific interest in the phenomenon has been continuous since that time.

Research with exploding wires grew rapidly in the years following World War II, fueled in part by the rapid growth of pulsed power technology and improvements in fast electrical and optical diagnostics, e.g., high-speed photography. Practical interest was generated by applications such as electric bridge wires for high-explosive detonator studies, the development of electrical fuses, the generation of high magnetic fields, and interest in plasmas for electrical power from fusion reactions¹. Chace surveyed the literature concerning exploding wire research in 1959 and, with Moore, edited the proceedings for a series of conferences on exploding wire research [3]. These publications provide a detailed summary of the "state of the art" through the late 1960s.

One reason for a high level of scientific interest is that exploding wires afford an opportunity to study a metallic element in all the states: solid, liquid, vapor, gas, and plasma. Among the many contributors to the scientific literature and to an increased understanding of some of the underlying physical phenomena was F. D. Bennett and his collaborators at the U.S. Army Ballistics Research Laboratory (BRL), one of the forerunners of the U.S. Army Research Laboratory (ARL). In the 1950s, problems with the high-speed flight of projectiles and renewed interest in plasmas revived interest in fluid mechanics, the principal research interest of the BRL group. Bennett [4] noted that the study of the shock waves and other flow patterns around exploding wires could provide useful information about analogous disturbances caused by high-velocity objects, such as meteorites and

¹Currently, there is renewed interest in this application. One of the more promising approaches to fusion power is the use of a pinched plasma to produce a burst of high-energy x-rays which, in turn, are used to compress a fuel pellet. Sandia National Laboratory in Albuquerque, New Mexico, a leader in exploding wire research for decades, uses hundreds of exploding wires to produce a pinched plasma for this purpose in a device called the Z machine. Progress with the Z machine was described in two recent articles: *Science News* 153, pp. 46-47, January 17, 1998 and *Scientific American* 279 No.2, p.40, August 1998.

missiles, traveling through the atmosphere. He and his colleagues applied the diagnostic techniques developed for research in aerodynamics using wind tunnels to study the many aspects of the exploding wire phenomena [5-7]. In this work and in almost all reported research with exploding wires, the wires were of uniform diameter. Any nonuniformity was the result of instabilities in the solid [8-10], liquid, or plasma phase [11]. These effects were observed as striations in flash x-ray pictures [12].

In some recent experimental work, Me-Bar and Harel [13] have investigated phenomena accompanying the explosion of segmented wires. They found that during most conditions, the wires exploded in a manner that was considerably different from that observed when smooth wires undergo similar types of explosions. In particular, the small-diameter segments exploded when expected, but the large-diameter segments did not. Indeed, the large segments were recovered relatively undamaged after the experiments. It was evident from the data, however, that current sufficient to explode the large segments continued to be conducted throughout the experiment. It was therefore conjectured that the explosion of the small segments produced a plasma arc that surrounded the large segments and provided an alternate path for the current.

An understanding of the manner in which segmented conductors explode or ablate is important for a number of physical applications. In Reference 13, the relevance to aircraft radomes, various types of circuit breakers, and a few other cases of practical importance was suggested. In addition, present efforts to effect the destruction of metallic (shaped charge) jets by electromagnetic fields [8] depend strongly on the assumption that current is conducted throughout the jet and not diverted by plasma arcs that might form when smaller diameter parts of the jet have vaporized. Similarly, in new designs of plasma igniters for electrothermal-chemical launchers [14], current is conducted through a periodic array of solid and plasma conductors, and it is important to understand what influences the manner in which the conduction occurs.

In this report, we are concerned with extending the work described in Reference 1. First, we report results of experiments on a variety of conductors of practical importance—namely, aluminum, copper, and brass; in Reference 13, all results discussed were for stainless steel wires. Second, we investigate the effect of the Lorentz or $\vec{J} \times \vec{B}$ force on the wire, once the explosion of the smaller segments has occurred. Examination of these data provides additional evidence to support the hypothesis in Reference 13 that current does not flow through the large segments after the explosion. Third, we present some model calculations in which the magnetic diffusion equation is solved in two dimensions and in the steady state for a periodic array of high-conductivity (solid) and low-conductivity (plasma) conductors. These calculations, although preliminary, do provide some insight into the possible conduction modes for this type of problem and provide parameters

that can be varied to influence those modes. The calculations also provide motivation for a final set of experiments in which we have physically confined the plasma in the vicinity of the exploded wire. Results of these experiments indicate a means by which the current can be forced to remain confined to the large-diameter segments.

The organization of the report is as follows. In Section 2, we describe the experimental setup. In Section 3, we discuss the experimental data for the various conductors studied. Section 4 contains the theoretical work (calculations) to which we alluded earlier. In Section 5, we describe results of experiments in which the plasma is confined in the radial direction. Finally, Section 6 contains a brief summary along with some suggestions for future work.

2. EXPERIMENTAL SETUP

The test setup for the experiments is shown schematically in Figure 1. The power source, not shown, is a 6.593 mF, 1.6 MJ capacitor bank. This bank consists of 32 parallel units, each of which contains a series combination of a 207- μ F energy storage capacitor, an energy-absorbing resistor, and two parallel coaxial cables. Each resistor is mounted on a capacitor terminal and is connected to the centers of the parallel coaxial cables. The center conductors of the 12.2-m-long cables are attached to the positive electrode (hot plate) of the test assembly; the coaxial cable shields are connected to the ground plate. Both plates are made of aluminum and are 800 mm wide by 685 mm high and 37 mm thick. They are held parallel for these tests at a spacing of 152 mm.

Replaceable copper test plates, 150 mm wide by 250 mm high by 3.2 mm thick, are attached to the tops of the aluminum plates. A 25-mm-diameter hole is located near the top center of each pair of test plates and is covered with a thin piece of aluminum foil. After the capacitor bank has been charged, the open circuit between the electrified and grounded test plates is closed by using a compressed air gun to launch the wire sample through the foil-covered hole and across the air gap. The arrival of the tip of the wire near the electrified plate initiates the current.

A set of three 450 kV x-ray tube heads was used to aid in test diagnosis. In order to expose three, non-overlapping images of the test wire on a single film, the tube heads are stacked vertically and aligned with the approximate center of the air space separating the parallel test plates. This orientation is shown in Figure 1. Each head has a projected line of sight (LOS) that is perpendicular to the flight path of the test wire. The x-ray heads are pulsed sequentially, starting with the middle tube head, then the top, and finally the bottom. The x-ray triggering sequence begins at the onset of current flow through the test wire and is initiated by the output signal from

a shielded Rogowski belt. This belt is buried in the grounded aluminum plate in such a way that it encloses the current from all 64 cables.

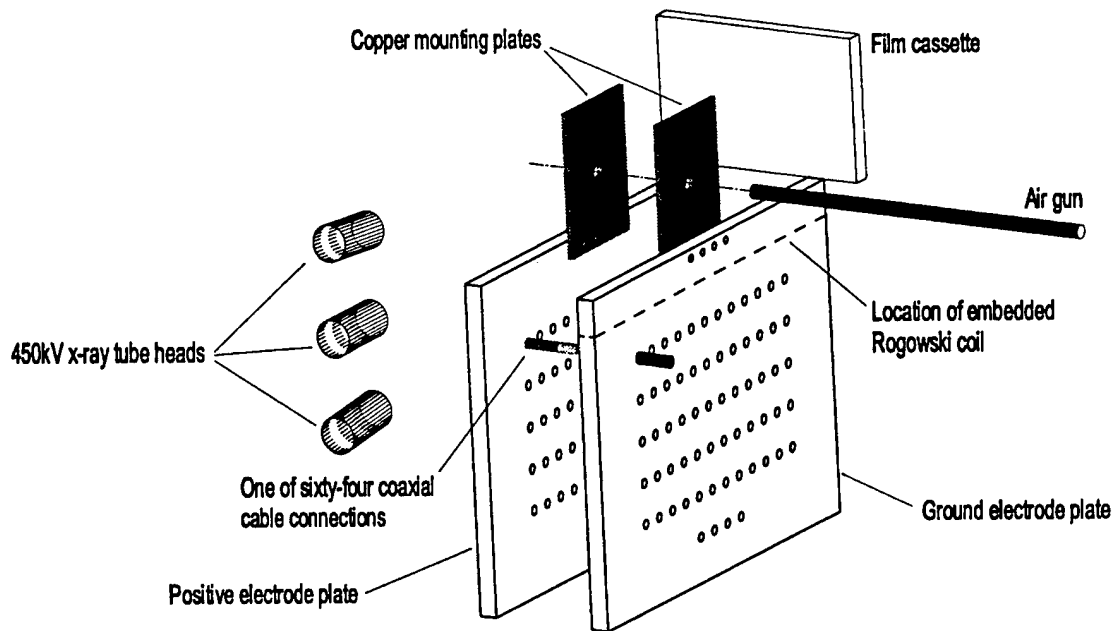


Figure 1. Experimental Setup for Shots S_{14} Through S_{22} .

An additional diagnostic is added to the capacitor bank to measure part of the current to the test stand. A 10-kilo-ohm ($k\Omega$) shunt resistor is connected in parallel with the energy-absorbing resistor of one of the 32 capacitors. The portion of the capacitor current that flows through the shunt is measured by a small Pearson coil placed around a heavily insulated lead. The output of this circuit is a voltage proportional to the current from this single capacitor. Both this circuit and the total Rogowski signal were calibrated in a separate, earlier experiment in which a large Pearson coil that measured the total circuit current was employed. A high-voltage probe, Tektronix Model P6015A, connected to the aluminum plates, is used to determine the time dependence of the voltage across the test assembly.

3. EXPERIMENTAL RESULTS

We discuss nine tests that were conducted on both segmented and smooth samples of copper, aluminum, yellow brass, and type 302 stainless steel wires. A summary of the characteristics of each test, indicating the geometry, the wire material, the charging voltage, and the x-ray times is presented in Table 1. The nominal dimensions of all the samples are shown in

Figure 2. In Appendix A, we describe some additional tests and present all the radiographs from the experiments with unconfined wires.

Table 1. Data for Shots S_{14} Through S_{22}

Test No.	Wire Material	Wire Geometry	Charge Voltage (kV)	X-Ray Flash Times (ms)		
				t_1	t_2	t_3
S_{14}	Brass	smooth	8.5	10	36	67
S_{15}	Brass	segmented	8.5	11.5	26.6	68.3
S_{16}	Copper	smooth	8.5	23.3	36.6	61.2
S_{17}	Copper	segmented	8.5	42.1	66.6	111.3
S_{18}	Aluminum	smooth	8.5	23.4	46.6	91.2
S_{19}	Aluminum	segmented	8.5	23.3	36.6	61.2
S_{20}	Copper	segmented	9.5	51.4	66.5	101.1
S_{21}	Stainless Steel	segmented	8.5	10.5	23.5	46.2
S_{22}	Stainless Steel	smooth	8.5	43.4	49.5	56.2

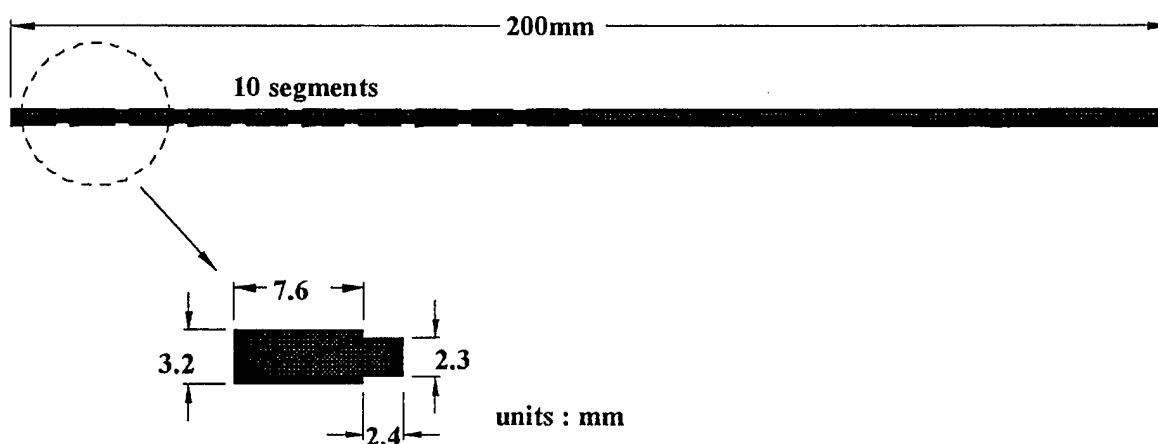


Figure 2. Dimensions of Samples Employed in Shots S_{14} Through S_{22} .

The x-ray results for a typical test (Test S_{15}), a segmented brass wire, are shown in Figure 3. The major vertical elements in this image are the replaceable copper plates; the thin vertical line near the center of the picture is a fiducial mark on the x-ray film cassette. The direction of motion of the wire is from right to left, or from ground plate to charged plate. The bottom image

shows that at $26.6\ \mu\text{s}$, the necks or small-diameter sections of the wire have exploded. The top image, at $68.3\ \mu\text{s}$ after current initiation, shows that the smooth section of the wire has exploded, whereas the residual segments of the same diameter have not. This result is consistent with those of Reference 13. The last segment of the wire has been accelerated into the adjacent segment at $68.3\ \mu\text{s}$ (the first of the ten segments is obscured by the charged plate). This phenomenon was also observed in Reference 13 where the joined segments or necks were recovered after some tests. Recovery of the segments was not possible in the experiments catalogued in Table 1 since those experiments were performed at an outdoor facility in an open geometry.



Figure 3. Radiographic Results for the Explosion of the Segmented Brass Wire in Shot S₁₅.

The current feed to the test plates in our experiments is asymmetrical. Consequently, a Lorentz force results, which acts on the test specimen to accelerate it vertically between the replaceable plates. The effect is barely discernible for the brass, aluminum, or stainless steel samples. For the copper samples, however, the larger action required to melt them, together with the presence of the Lorentz force, results in an upward acceleration of the smooth part of the wire.

This effect is shown in Figure 4 (S₁₇ in Table 1). The bottom image shows that the smooth part of the wire has a small kink near the center of the segment. As is suggested subsequently,

this bending probably arises because the current density, and thus the Lorentz force, is higher near the center of such a segment than it is at the ends. In the top image, the smooth wire has separated at this point but only after considerable deflection in the vertical direction. The residual segments from the front of the wire, although having the same diameter as the smooth wire and much lower mass, experience only small vertical deflections. This behavior suggests that little current is conducted through those pieces. These images substantiate the following conclusions reported in Reference 13: (1) Current is diverted around the large-diameter segments that remain after the smaller diameter region explodes; (2) the segment nearest the smooth wire section appears to behave partially as a smooth section and partially as a neck or bead; (3) the segment nearest the smooth section is accelerated toward its nearest neighbor (other segments also show the same behavior).

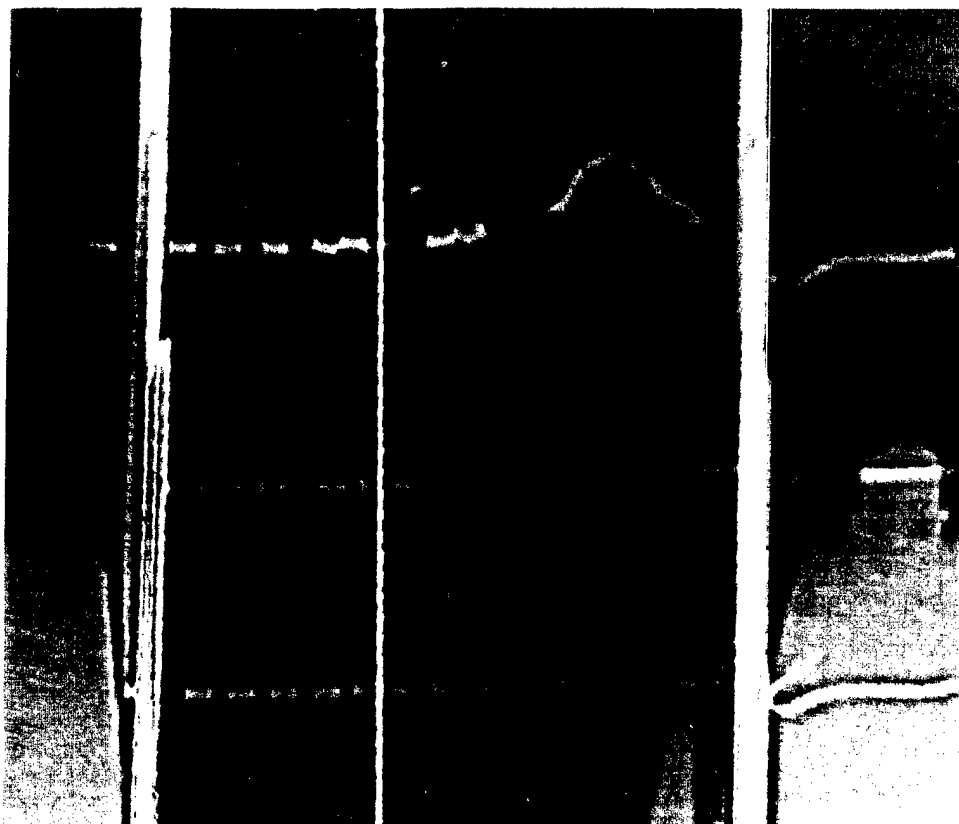


Figure 4. Radiographic Results Demonstrating Acceleration by the Lorentz Force for the Copper Wire in Shot S₁₇.

The behavior in the tests of smooth wires was, except for the copper samples, similar to that reported in Reference 13. All those samples exploded when expected and for the reasons noted previously. The electrical data, viewed in conjunction with the x-rays, can be used to infer approximate times for the occurrence of the significant events in the test.

Figure 5 shows some of the electrical data for Shot S₁₅. Both the current I and the derivative of the current dI/dt demonstrate essentially the same behavior for all the samples studied except copper. The time of explosion of the necks can be identified by the sharp spike in the derivative of the current signal at approximately 23 μs . The time of explosion of the smooth section of the wire is not so readily discernible as for the neck, but it probably occurs near the small peak at about 53 μs .

The voltage drop across the wire $V(t)$ consists of two components and is given by

$$V(t) = L \frac{dI}{dt} + IR(t), \quad (1)$$

in which I is the circuit current, L is the inductance of the test fixture, and R is the resistance of the wire. This relationship is based on the assumption that L does not change with time, an approximation that is good for our test stand even after the wire begins to explode. Since all the quantities in Equation (1), except $R(t)$, are either known or measured in the test, a time-dependent resistance can be inferred from the data.

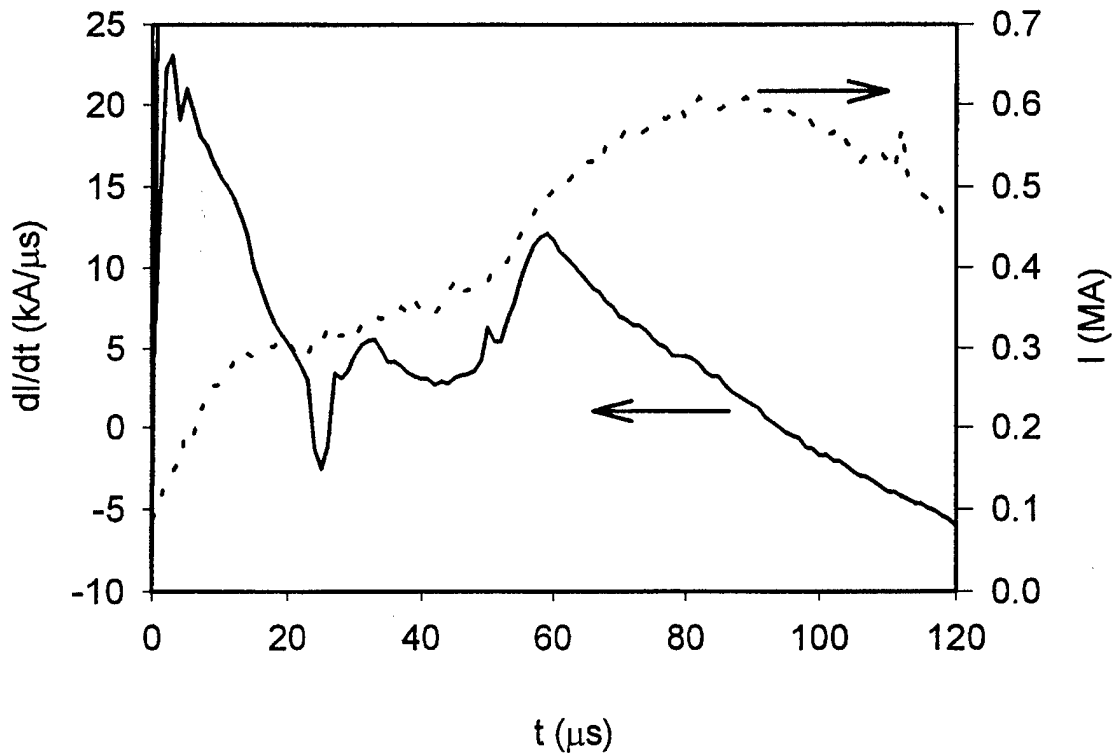


Figure 5. Current I (dotted curve) and Time Derivative dI/dt (solid curve) for Shot S₁₅.

The resistance R so determined is shown in Figure 6 for Shot S_{14} , a smooth wire, and for Shot S_{15} , a segmented wire. In Shot S_{14} , the explosion of the heated, highly resistive, smooth wire leads to an abrupt transition to a low value of resistance governed by the properties of the plasma that exists between the copper plates. For the segmented wire, however, the behavior is more complex and can be explained as follows. If the arc resistance at the connection between the wire and the copper plate is ignored, the quantity $R(t)$ is composed of two series resistors. Since heat transfer between the necks and segments occurs on a time scale that is much slower than that of the experiment, the necks and smooth sections are at different temperatures and have different resistance. The peak at about $23\ \mu\text{s}$ corresponds to the rapid rise in temperature of the necks just before explosion. After explosion, the resistance drops. A number of complex phenomena coexist in the region from 25 to $60\ \mu\text{s}$. Resistance is decreasing because of the diversion of current around the heated segments, presumably into a plasma. At the same time, the resistance of the smooth section continues to rise as this section approaches the vaporization point. The net result of this competition is that, for a segmented wire, the explosion of the smooth portion, which occurs at approximately $55\ \mu\text{s}$, produces an electrical signature that is weaker than that of either a neck or a continuous smooth wire.

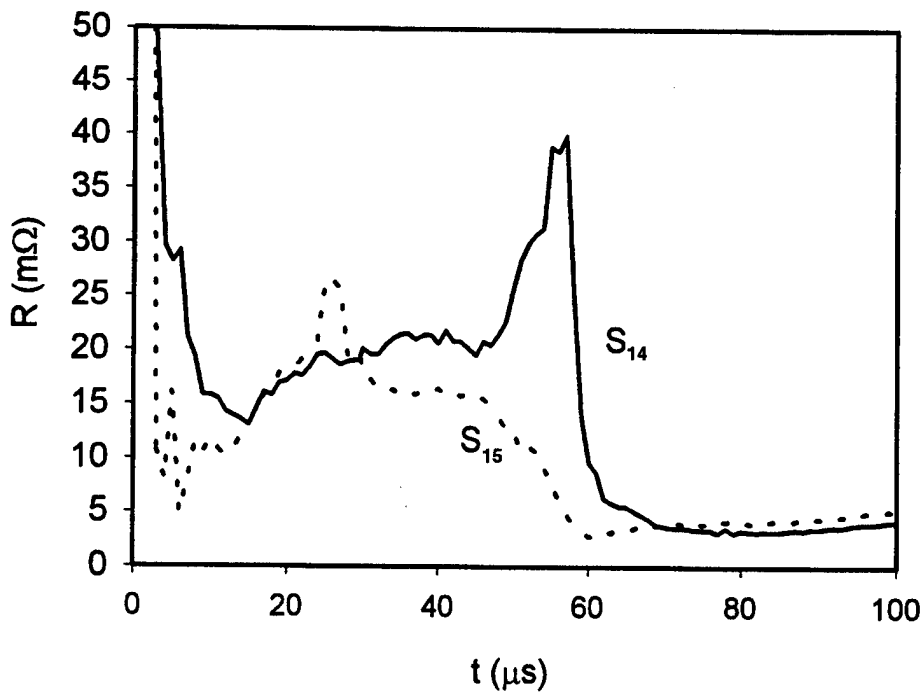


Figure 6. Resistance Versus Time for Shot S_{14} , Corresponding to a Smooth Wire (solid curve), and Shot S_{15} , Corresponding to a Segmented Wire (dotted curve).

4. CALCULATIONS

The conclusion that current is diverted away from small-diameter segments of wire and into the plasma created by the explosion of the small segments is rather counterintuitive. Even at high temperatures, the conductivity of the resulting plasma is always several orders of magnitude smaller than that of the remaining solid segments. Furthermore, there is insufficient mass in the small-diameter segments or time in the experiment for the plasma to expand to an area sufficiently large to account for the difference in the conductivities.

In order to help elucidate the effect, we have undertaken some simple model calculations. The model that has been employed is shown schematically in Figure 7a. A series of solid conductors, which represent the large-diameter segments that remain after the explosion of the smaller segments, is denoted by the solid black rectangles. These conductors are separated by a series of plasma arcs and extend above and below the regions indicated in Figure 7a. Ultimately, they terminate at electrodes, not shown in Figure 7a. There is also plasma in the region located to the right of the solid conductors and extending to the plane $r = r_m$ as indicated. The plasma is simply represented by an immobile, low-conductivity substance. The entire configuration is assumed to be axisymmetrical so that there is no dependence on the azimuthal angle θ . A total current i_0 is conducted from the lower to upper electrode through the various conductors.

To further simplify the model, we make the assumption that there is a large number of solid-plasma conductors and that far away from the electrodes, each sequence of conductors will obey approximately periodic boundary conditions. Consequently, it is only necessary to study one combination. If we select the part bound by the lines L_1 and L_2 in Figure 7a, we can argue from symmetry that $\partial B/\partial z = 0$ along these lines. The domain of the calculation therefore will be taken to be the region shown in Figure 7b. In this figure, we have taken L_1 to be at $z = 0$ and L_2 to be at $z = z_m$ and have denoted by r_s and z_s the radius and the half-height of the solid segments, respectively. Clearly, r_m is a measure of the lateral extent of the plasma, and z_m is a measure of the vertical separation between similar segments in the periodic array.

We assume that the solid conductors have constant electrical conductivity σ_s and that the plasma has constant conductivity σ_p . The assumption that the two conductivities are constant is not required in either the model or the calculations but is made in the interest of simplicity. A more realistic assumption is not expected to affect the qualitative conclusions reached. Furthermore, since we are interested in situations in which σ_s is large compared to σ_p , we will assume that it is infinite. Earlier calculations [14] that we have made in which σ_s was large but finite produced virtually identical results. The conduction paths through the domain can be determined by solving

the magnetic diffusion equation. For the axisymmetrical geometry being considered, that equation can be written

$$\mu\sigma \frac{\partial B}{\partial t} = \frac{\partial^2 B}{\partial r^2} + \frac{1}{r} \frac{\partial B}{\partial r} + \frac{\partial^2 B}{\partial z^2} - \frac{B}{r^2} - \frac{1}{\sigma} \frac{\partial \sigma}{\partial r} \frac{\partial B}{\partial r} - \frac{B}{\sigma} \frac{\partial \sigma}{\partial r} - \frac{1}{\sigma} \frac{\partial \sigma}{\partial z} \frac{\partial B}{\partial z} \quad (2)$$

Here, B denotes the one surviving component of the magnetic induction (the θ component) and μ denotes the magnetic permeability.

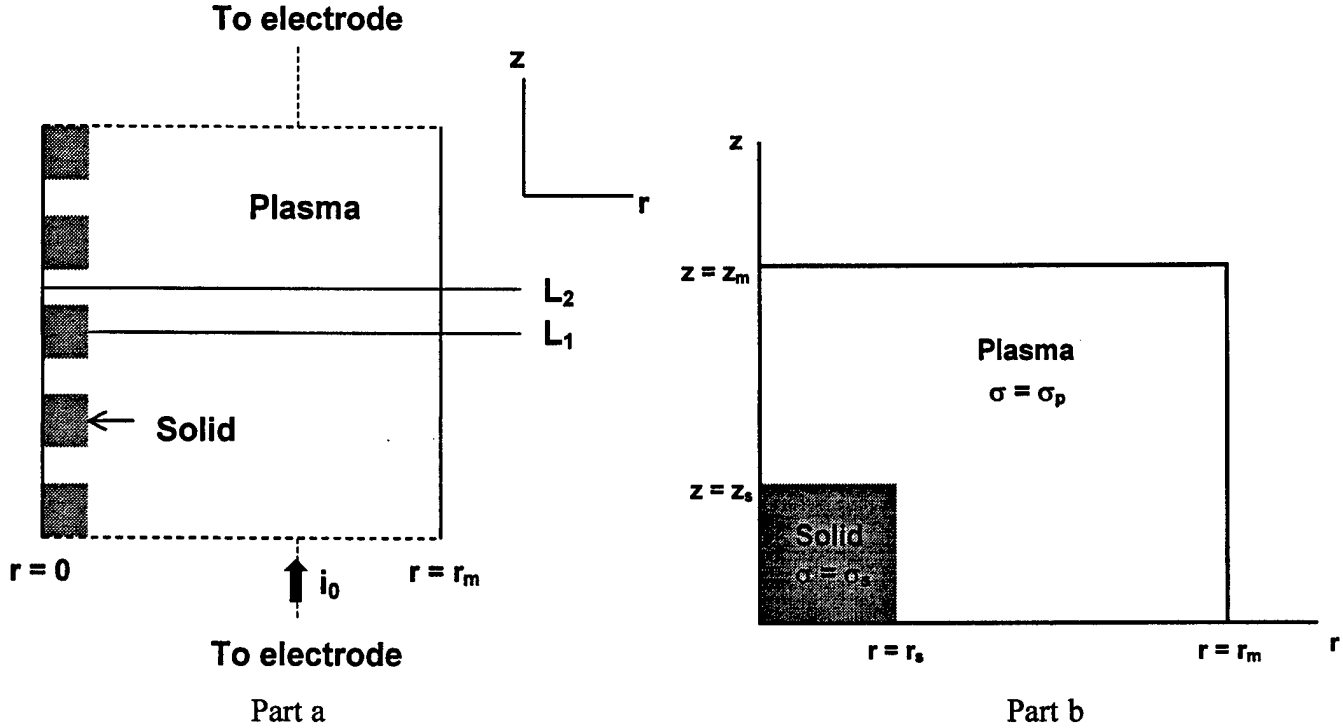


Figure 7. Model Employed in Calculations: (a) a Periodic Array of Cylindrically Symmetrical, Solid and Plasma Conductors; (b) the Calculation Domain That Lies Between Lines L_1 and L_2 in Part (a).

Equation (2) must be solved, subject to the boundary conditions

$$\begin{aligned} B(r = 0) &= 0, \\ B(r = r_m) &= \frac{\mu i_0}{2\pi r_m}, \end{aligned} \quad (3)$$

and

$$\left(\frac{\partial B}{\partial z} \right)_{z=0} = \left(\frac{\partial B}{\partial z} \right)_{z=z_m} = 0.$$

At all interfaces between the plasma and solid, we must also have

$$\hat{n} \times \frac{1}{\sigma} (\nabla \times \vec{B}) = 0, \quad (4)$$

in which \hat{n} denotes the unit normal to the surface. If this condition were not assured, the associated electric field would produce an infinite current in the perfectly conducting solid.

We have solved Equation (2) numerically for a number of interesting cases. The solutions were always computed until a steady state was reached. It is evident that in the steady state and under the assumptions of constant conductivity in the plasma and infinite conductivity in the solid, the results depend entirely upon geometry and not upon the conductivity σ_p . Furthermore, if we normalize B by $\mu_0/(2\pi r_m)$ and the various dimensions by r_s , we can remove the explicit dependence on those parameters. We use this normalization in the remainder of the analysis and denote the normalized quantities by overbars. The accuracy of the numerical solutions was checked by reducing the grid spacing until no further change in the results was observed. Some comparison was also made with exact analytical solutions [14] that can be obtained in the one-dimensional limit.

Results from the two calculations of greatest interest are shown in Figure 8a and 8b. Plotted in each case are contours where the streamline function $\Psi = r \bar{B}$ is constant. For cylindrical, axisymmetrical geometry, it is possible to prove from Maxwell's equations that current is conducted along lines that are parallel to those contours. There are 11 such contours (including the extreme values of zero and unity) in each graph so that 10% of the total current is contained between successive contours. The contours are referred to as "current streamlines." The black rectangles in each of the figures represent the area bound by the solid conductor.

The calculation in Figure 8a corresponds to a situation in which \bar{r}_m is large compared to \bar{z}_m . For this case, it is apparent that the results are almost one-dimensional with the current fairly uniformly distributed along the r axis and a relatively small amount of current contained in the solid. This behavior occurs even though the solid has infinite electrical conductivity. For the opposite limiting case, namely, when \bar{z}_m is large compared to \bar{r}_m , much different behavior is observed as is shown in Figure 8b. For this case, most of the current is conducted in the solid.

Our understanding of these different results can be described approximately as follows. If there is a relatively large region where no solid exists, such as in the upper half of the domain for the two cases just described, then the current will tend to diffuse across this low-conductivity

region. Consequently, the streamlines indicate a fairly uniform distribution of current along $\bar{z} = \bar{z}_m$. In each case, the current will traverse the domain from bottom to top in such a way as to minimize the resistance experienced in the low-conductivity regions. For the case $\bar{r}_m \ll \bar{z}_m$, the preferred path is across the arc in the horizontal direction since this direction corresponds to the smaller distance and greater cross-sectional area. However, for $\bar{r}_m \gg \bar{z}_m$, the shorter length, greater area path is in the vertical direction. Thus, for $\bar{r}_m \gg \bar{z}_m$, virtually no current is present in the solid even though its conductivity is infinite.

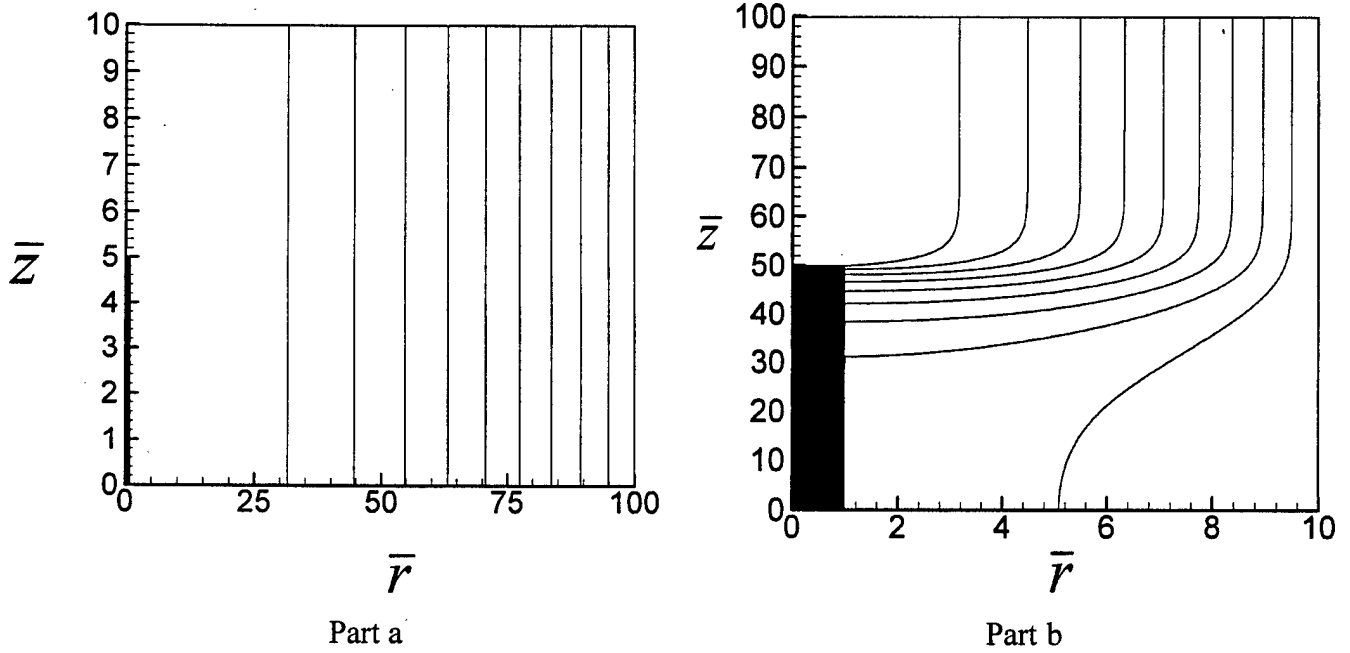


Figure 8. Current Streamlines in Calculation Domain for Two Limiting Cases: (a) $\bar{r}_m \gg \bar{z}_m$; (b) $\bar{r}_m \ll \bar{z}_m$.

Although we do not present the results, we have also performed calculations for other aspect ratios and for other values of \bar{z}_s . It is found, as expected, that for aspect ratios between the two extreme cases just studied, there is an intermediate amount of current in the solid. Furthermore, as \bar{z}_s increases, so too does the relative amount of current in the solid. Finally, as \bar{z}_s approaches unity, so that there is a continuous solid throughout the domain, the obvious one-dimensional result that predicts all the current in the solid and none in the plasma is obtained.

For typical segmented wire experiments, we have computed the mass present in the small segments and estimated the distance r_m to which the plasma would expand before being confined by the magnetic pinch forces. Generally, this distance is large compared to the segment separation so that the situation corresponding to that in Figure 8a is obtained. Consequently, it

is for these reasons that the current is diverted away from solid segments in the experiments performed. The results do suggest, however, that if the plasma could be confined mechanically to a relatively small value of r_m , results similar to those observed in Figure 8b would occur. In the following section, we describe experiments in which the plasma was confined about the axis of the wire with a Lexan sleeve.

5. EFFECTS OF PLASMA CONFINEMENT

The setup for the plasma-confinement experiments is somewhat different from that in which the plasma was allowed to expand freely. First, the experiments were performed in an indoor facility with a different power supply from that used previously. Second, a fixed wire, rather than one moving at low velocity, was employed. This change was made because the low-velocity launch used in the experiments with unconfined wires usually results in a wire trajectory that is not completely perpendicular to the test plates. If the same setup were used in a confinement experiment, either a complex launch package that includes the confinement apparatus or an extremely accurate launch into a fixed confinement apparatus would be required. These difficulties can be avoided through the use of a fixed wire geometry. Furthermore, since the motion of the wire is of minimal importance, no significant differences are expected between these experiments and ones in which the wire can move.

The power supply used in the experiments is a 20-kV, 1600- μ F capacitor bank, consisting of eight 200- μ F capacitors connected through 16 coaxial cables to a spark gap switch. The trigger generator for the spark gap produces a 75-kV pulse from which the capacitor bank must be protected; a magnetic switch configured in a coaxial arrangement provides this protection. The total current, I , is measured with a large Pearson coil that is threaded by the output current from the capacitor bank at the location of the magnetic switch. The switched output from the bank is connected through 16 coaxial cables to the periphery of two large aluminum plates, each of which is an octagon approximately 381 mm on a side (see Figure 9). Alternate sections of the octagonal periphery serve as the connection point for four of the cables. In this manner, an approximately symmetrical current feed is achieved so that the Lorentz force is minimized.

The center of the aluminum plates is milled so that a 15.2-mm by 22.9-mm replaceable brass plate can be mounted in the center of the test fixture. Mechanical brass fixtures soldered to the replaceable plates provide a means of clamping the specimen in the center of the test fixture. After the bank is charged, the spark gap switch is command triggered to initiate current through

the wire. A non-integrating, shielded Rogowski coil, embedded in the ground plate, measures the derivative of the total current, dI/dt .

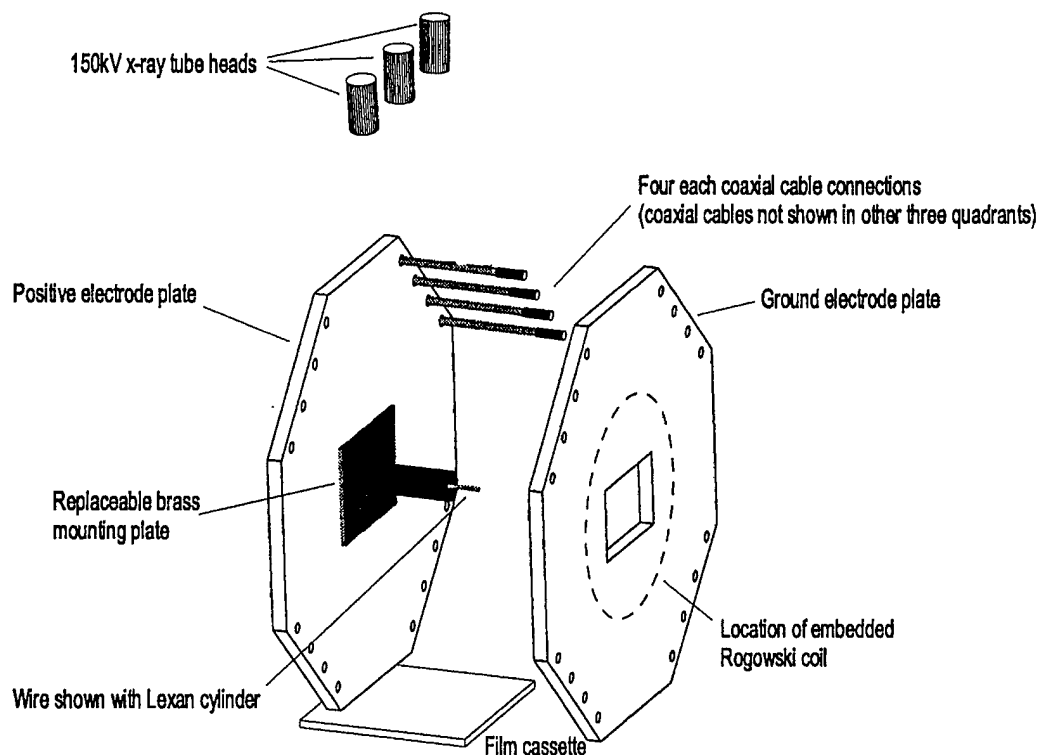


Figure 9. Experimental Setup for Plasma-Confinement Experiments.

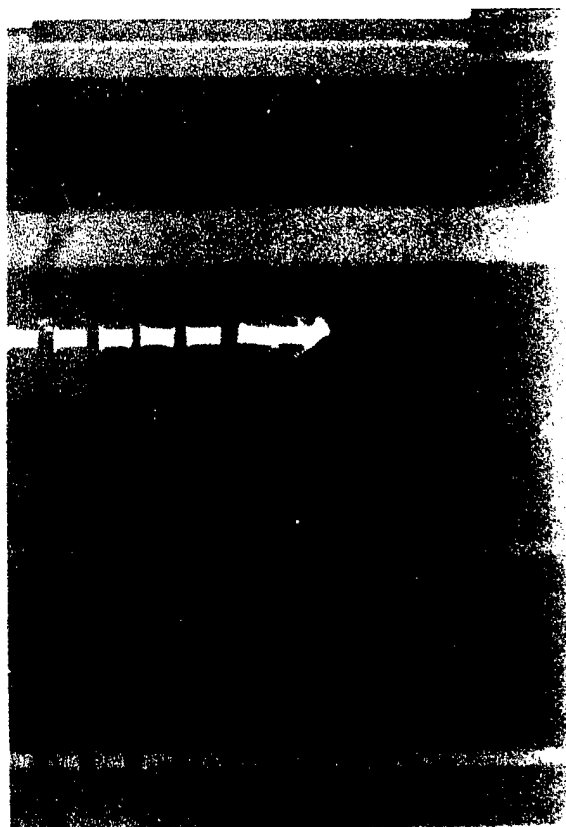
The x-ray coverage is similar to that of the unconfined experiments. In this case, three 150-kV x-ray tube heads are used. The tube heads are located directly overhead from the test fixture but are displaced so as to provide three non-overlapping images of the wire on a single strip of film. The x-ray timing sequence is slaved to the trigger pulse for the capacitor bank.

Tests were conducted with wire samples fabricated from a fuming bronze material used for welding rods. The principal constituent is copper. The pertinent data for this series of tests are summarized in Table 2. Tests T_1 and T_2 reconfirm the essential results described in Section 1 and employed the same wire geometry as in the earlier tests; it is denoted as "geometry 1" in the table. Figure 10a shows the x-ray images for test T_2 at a charge voltage of 16 kV. This voltage produces approximately the same levels of current as used in the unconfined experiments. The same effects reported in Section 1 are also observed in these tests.

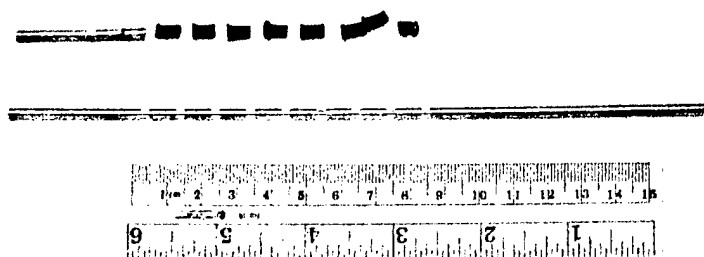
Since these tests are performed in an indoor facility, unexploded smooth-wire segments can be recovered following this experiment. Figure 10b is a photograph of the segments in what is

Table 2. Data for Shots T_1 Through T_5 .

Test No.	Wire Geometry	Lexan Inner/Outer Diameter (mm)	t_1	t_2	t_3
T_1	Smooth	Not applicable	20.7	80.0	120.0
T_2	Geometry 1	Not applicable	25.1	45.1	130.0
T_3	Geometry 2	Not applicable	22.1	40.1	100.0
T_4	Geometry 2	25.4/15.9	25.1	58.1	100.0
T_5	Geometry 2	38.1/15.9	60.0	80.1	100.0



Part a



Part b

Figure 10. Experimental Results for Test T_2 : (a) X-ray Images; (b) Photograph of Recovered Segments.

believed to be the same order as their appearance in the x-ray image. Most of the observations reported by the authors of Reference 13 are confirmed in these photographs. As previously, we observe that segments other than the initial one near the smooth wire are accelerated toward their nearest neighbor. Although it is not evident in Figure 10b, the end of the smooth section of wire nearest the segments shows the cratering described in Reference 1.

The analysis described in the preceding section was used to select the parameters for the confinement experiments. The critical parameters are the lengths of both the necks and adjoining smooth sections and the ratio of the diameter of the confinement wall to that of the smooth wire. The geometrical parameters and the material selected for confinement represent a compromise among several competing factors. Difficulty in machining the wire sample, the availability of confinement materials, and the ease of taking x-rays through the confinement structure are prominent among these factors. The dimensions chosen are shown in Figure 11, and the geometry is referred to as "geometry 2" in Table 2. The use of longer smooth-wire sections in these experiments permitted the inclusion of only two such segments within the electrified gap defined by the plates.

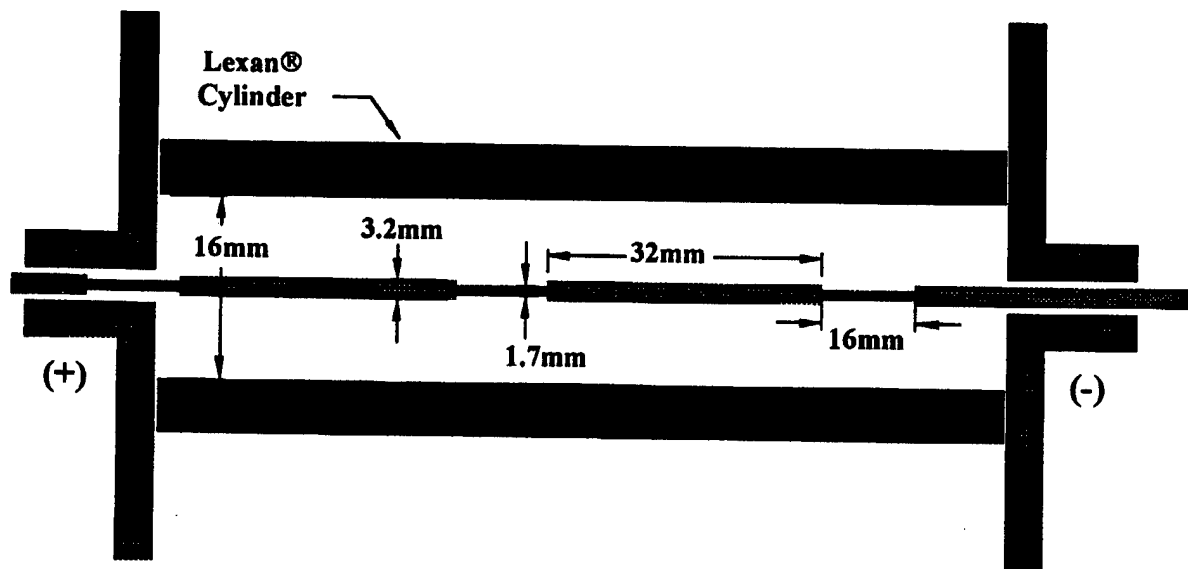


Figure 11. Wire Dimensions and Geometry for Plasma-Confinement Experiments.

Figure 12 shows the results of a calculation similar to those described earlier but for the selected dimensions. Specifically, the plasma is assumed to be confined within a radial distance of about 8 mm, and the various wire segments have the lengths and diameters shown in Figure 11. Clearly, the theory predicts that most of the current is contained in the large-diameter solid

segments near the center of the segments (i.e., at $z = 0$ in the figure) but that it “splits off” into the plasma as the ends of the segments are approached. Nonetheless, it is expected that these segments will probably explode in the experiment.

The behavior observed in test T_3 , in which there was no confinement structure, is identical to that reported for segmented wires in the preceding section. The two smooth sections between the necks were recovered after the test. The test shows that, as in the previous shots, there is sufficient expansion of the plasma to divert the current from the solid segments.

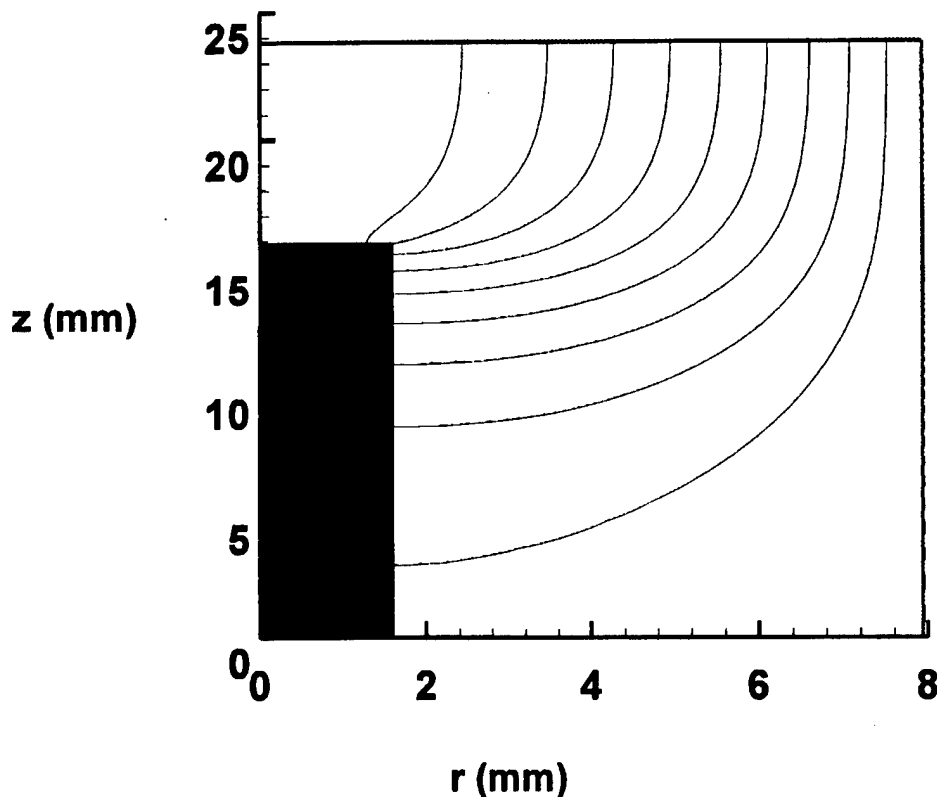
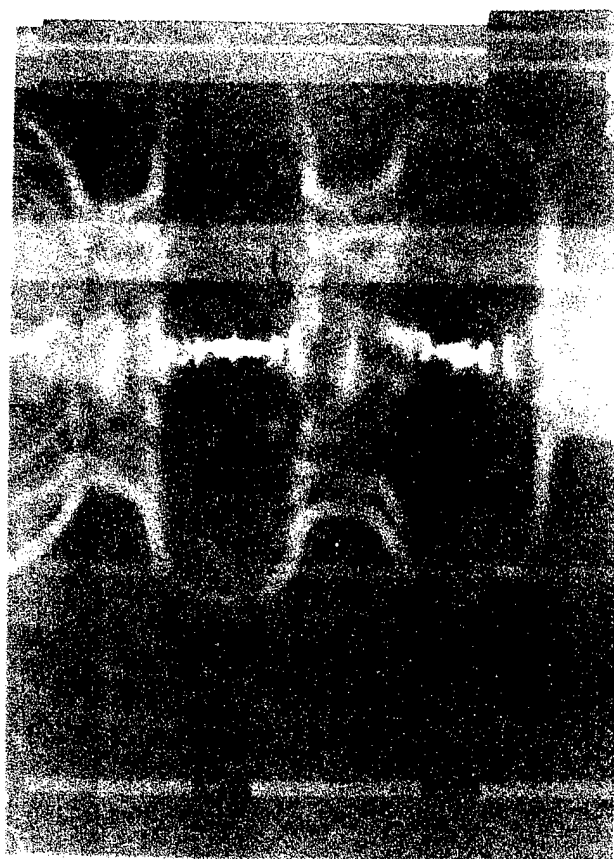


Figure 12. Calculated Current Streamlines for the Geometry Employed in the Plasma-Confinement Experiments.

For the two final tests in this series, a segmented wire of the same dimensions as in test T_3 and a confinement wall consisting of a Lexan tube with the dimensions given in Table 2 were employed. Enhanced x-ray images of the wire in both tests (T_4 and T_5) are shown in Figure 13. Clearly, the entire wire has exploded or is in the process of exploding. In Figure 13a, the outline of the confinement structure is faintly visible in the first (middle) and second (bottom) images. In the final image (top), the Lexan walls have expanded considerably and material has begun to accumulate in the smaller diameter region of the wire. In the left-most neck region, there is evidence of “splash”

from the collision of fragments from the ends of the segments that have been accelerated into each other. It should be observed that the region of lowest material density in this image is at the approximate centers of the smooth sections. This occurrence suggests that this part of the segment explodes before the ends and agrees with the model prediction that the center of the segments carries the most current.

Figure 13b also shows the results from test T_5 . This test was similar to test T_4 but employed a thicker confinement structure (see Table 2). The top image in Figure 10b shows that the entire wire explodes; the bottom image shows that the middle of the smooth sections explodes before the ends, as was suggested in the discussion of Figure 13a. Both results agree with inferences from our earlier calculations. It is also interesting to note that because of parallax effects from the x-ray geometry, several rings of matter density, reminiscent of "smoke rings," can be seen. The existence of these rings, well known from earlier experiments with exploding wires, has also been observed in experiments [15] in which shaped charge jets are heated by electrical currents.



Part a



Part b

Figure 13. Radiographic Results From Plasma-Confinement Experiments: (a) Test T_4 (thin walled Lexan sleeve); (b) Test T_5 (thick walled Lexan sleeve).

6. SUMMARY AND CONCLUSIONS

We have performed both experiments and calculations to determine the electrical conduction characteristics of exploding segmented wires. In the first set of experiments, the plasma resulting from the explosion of the small-diameter necks was allowed to expand freely around the wire; in the second set, the plasma was confined in its radial dimension. The experiments were explained and in some cases motivated by calculations in which the magnetic diffusion equation was solved to predict the preferred conduction pathways for the various configurations.

General conclusions from the work can be described as follows.

a. For typical wire geometries, the plasma produced by the explosion of the small-diameter segments expands sufficiently to divert current from the remaining large-diameter segments. Consequently, the large segments do not explode, despite the action being sufficient to produce explosion if all the current were carried by those segments.

b. For situations when the plasma is confined mechanically in the radial direction, insufficient expansion occurs to divert the current. In those cases, the large-diameter segments explode; the explosion occurs first in the center of the segments and later at the ends.

c. Calculations in which the magnetic diffusion equation was solved for a perfectly conducting solid, surrounded by constant conductivity plasma, predict the length scales relevant to the problem. If the plasma expands to a distance that is large compared to the segment separation, current will be diverted away from the segment; in the opposite limiting case, current will be confined to the solid. The theory also predicts that current concentration is greatest near the center of segments, and consequently, if explosion occurs, it should occur at the center before it does at the ends. This prediction agrees with the experimental results.

Future work on the theoretical aspects of this problem should be concerned with including details of the plasma properties. It would be especially worthwhile to evaluate the plasma temperature and spatial dependence of the conductivity. Although the qualitative conclusions reached earlier are not expected to change, the quantitative details might be affected. Future experimental work should address the problem of providing for plasma confinement in practical applications where current diversion is an undesirable consequence of the explosion.

REFERENCES

1. Chace, W.G., "A Brief Survey of Exploding Wire Research," in *Exploding Wires*, edited by Chace, W.G. and Moore, H.K., (Plenum Press, New York, 1959), Vol. 1, p 7.
2. Anderson, J.A., Proc. National Academy of Science U.S., **6**, pp. 42-43 (1920). See also references cited in reference 1.
3. *Exploding Wires*, edited by Chace, W.G. and Moore, H.K., (Plenum Press, New York) Vol. 1 (1959); Vol. 2 (1962); Vol.3 (1964); Vol. 4 (1968).
4. Bennett, F.D., "Exploding Wires," Scientific American, **206** No. 2, p 103, 1962.
5. Bennett, F.D., "Cylindrical Shock Waves From Exploding Wires," Ballistics Research Laboratory Report No. 1035, April 1958.
6. Bennett, F.D., "High Temperature Exploding Wires," Ballistics Research Laboratory Report No. 1339, October 1966.
7. Bennett, F.D., Burden, H.S., and Shear, D.D., "Expansion of Superheated Metals," Journal of Applied Physics, **45**, No. 8, p. 3429, August 1974; Ballistics Research Laboratory Report No. 1686, November 1973, and references therein.
8. Littlefield, D.L., and Powell, J.D., "The Effect of Electromagnetic Fields on the Stability of a Uniformly Elongating Plastic Jet," Phys. Fluids **A 2**, No. 12, 2240, December 1990; Ballistics Research Laboratory Report BRL-TR-3108, June 1990.
9. Littlefield, D.L., "Thermomechanical and Magnetohydrodynamic Stability of Elongating Plastic Jets," Phys. Fluids **6** (8), 2722 (1994).
10. Powell, J.D., "The Effects of Electromagnetic Fields on the Stability of Shaped Charge Jets in Walker-Plate Experiments"(U), U.S. Army Research Laboratory Report ARL-TR-1153, July 1996 (SECRET).
11. Kalanar, D.H., and Hammer, D.A., "Observation of a Stable Dense Core Within an Unstable Coronal Plasma in Well-Initiated Dense Z-Pinch Experiments," Phys. Rev. Lett., **71**, No. 23, 3806, December 1993.
12. Fansler, K.S., and Shear, D.D., "Correlated X-Ray and Optical Streak Photographs of Exploding Wires," *Exploding Wires*, edited by Chace, W.G., and Moore, H.K., (Plenum Press, New York, 1968), Vol. 4, p. 185.
13. Me-Bar, Y., and Harel, R., Journal of Applied Physics, **79**, 1864 (1996).

14. Powell, J.D., Thornhill, L.D., and Batteh, J.H., IEEE Trans. Magn (in press). See also J.D. Powell, L.D. Thornhill, and J.H. Batteh, U.S. Army Research Laboratory Report No.1436, 1997.
15. Bruchey, W.J., Filbey, G.S., Hollandsworth, C.E., Hummer, C.R., Keele, M.J., and Kleponis, D.J., experimental data (unpublished).

APPENDIX A

DIGITIZED RADIOGRAPHS FOR ALL TESTS
WITH UNCONFINED WIRES

INTENTIONALLY LEFT BLANK

DIGITIZED RADIOGRAPHS FOR ALL TESTS WITH UNCONFINED WIRES

In previous reports, we have discussed some of the similarities between the appearance of the fragments from electrically exploded wires and shaped charge jets (SCJs) subjected to electric currents. These are fundamentally different physical systems. Initially, the wire is a completely stable system whereas a propagating SCJ is inherently unstable and particulates into numerous fragments eventually. Moreover, the entire wire is heated simultaneously while segments of the moving jet are heated sequentially. Nonetheless, we have observed in numerous radiographs that the fragments from both processes evolve eventually into hollow rings of matter density that resemble "smoke rings." Similar structures were observed in the debris of exploded wires in experiments conducted in the 1950s.

Computational studies of SCJ heating [A-1 through A-3] predict a sequence of different fragment shapes at different times after an SCJ exits an electrified plate structure. Many of these shapes have been observed in the ARL experiments reported by Filbey et al. [A-4], Hummer and Hollandsworth [A-5], and Keele et al. [A-6].

Joule heating, which eventually causes conductors to explode, varies with the inverse fourth power of the radius. This dependence coupled with small imperfections in the wire diameter suggests that a single x-ray flash of an exploding wire can capture fragments at many different times following the explosion. Although many other physical phenomena accompany the vaporization of a wire, the diameter variations in the wire in conjunction with Joule heating are certainly principal factors in producing the observed striations in x-ray pictures. To emphasize this, we performed some additional experiments, not tabulated in Table 1, where radius variations along the wires were deliberately introduced.

These additional tests, along with the data from Table 1, are included in Table A-1. All the radiographs from the experiments with unconfined exploding wires are shown on the succeeding pages. These radiographs provide a number of examples of striations similar to those reported in the earlier exploding wire literature.

A first attempt to confine the plasma resulting from explosion of the necks was made in Shot S₂₄. A Lexan sleeve, 3.18 mm diameter and 0.79 mm in thickness, was used to enclose a segmented brass rod. This attempt failed, as the x-ray for this test shows. The Lexan walls were too thin and the explosion of the necks destroyed the sleeve.

Table A-1. Data for Shots S₁₃ Through S₂₄

Test Sample	Wire Material	Wire Geometry	Charge Voltage (kV)	X-Ray Flash Times (ms)		
				t1	t2	t3
S ₁₃	Brass	smooth	8.5	n/a	n/a	n/a
S ₁₄	Brass	smooth	8.5	10	36	67
S ₁₅	Brass	segmented	8.5	11.5	26.6	68.3
S ₁₆	Copper	smooth	8.5	23.3	36.6	61.2
S ₁₇	Copper	segmented	8.5	42.1	66.6	111.3
S ₁₈	Aluminum	smooth	8.5	23.4	46.6	91.2
S ₁₉	Aluminum	segmented	8.5	23.3	36.6	61.2
S ₂₀	Copper	segmented	8.5	51.4	66.5	101.1
S ₂₁	Stainless Steel	segmented	8.5	10.5	23.5	46.2
S ₂₂	Stainless Steel	smooth	8.5	43.4	49.5	56.2
S ₂₃	Brass	sawtooth	8.5	32.5	37.5	61.1
S ₂₄	Brass	segmented	8.5	32.3	52.7	61.2

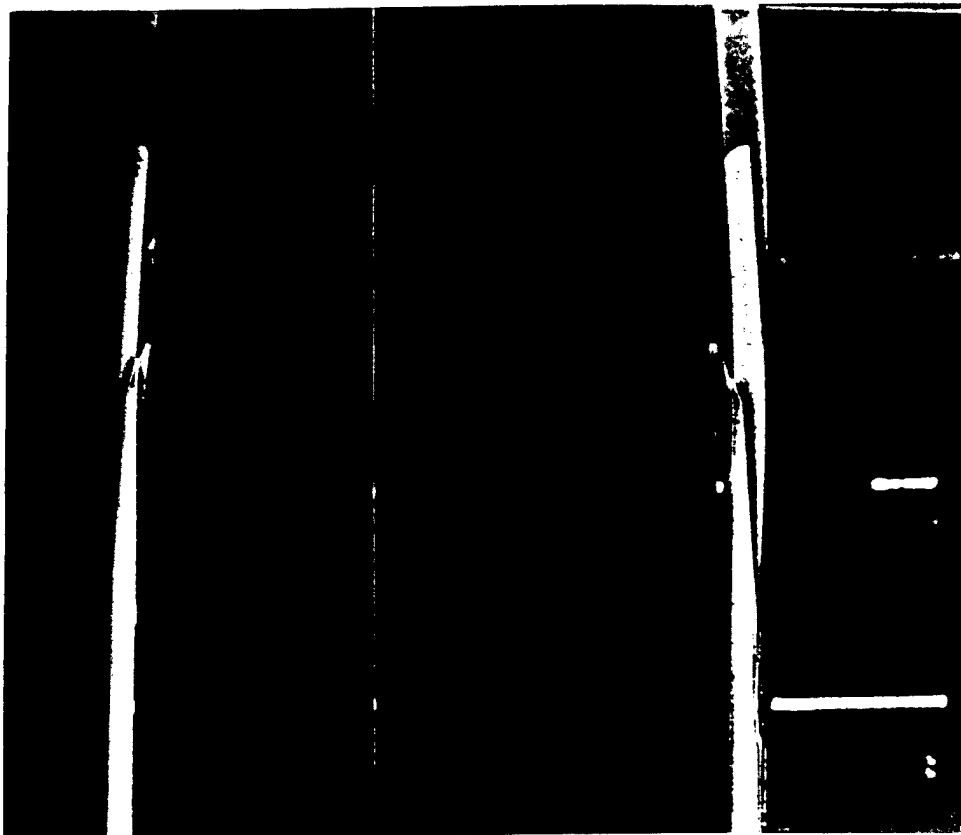


Figure A-1. Radiograph of Shot 14: Smooth Brass Wire.



Figure A-2. Radiograph of Shot 15: Segmented Brass Wire.

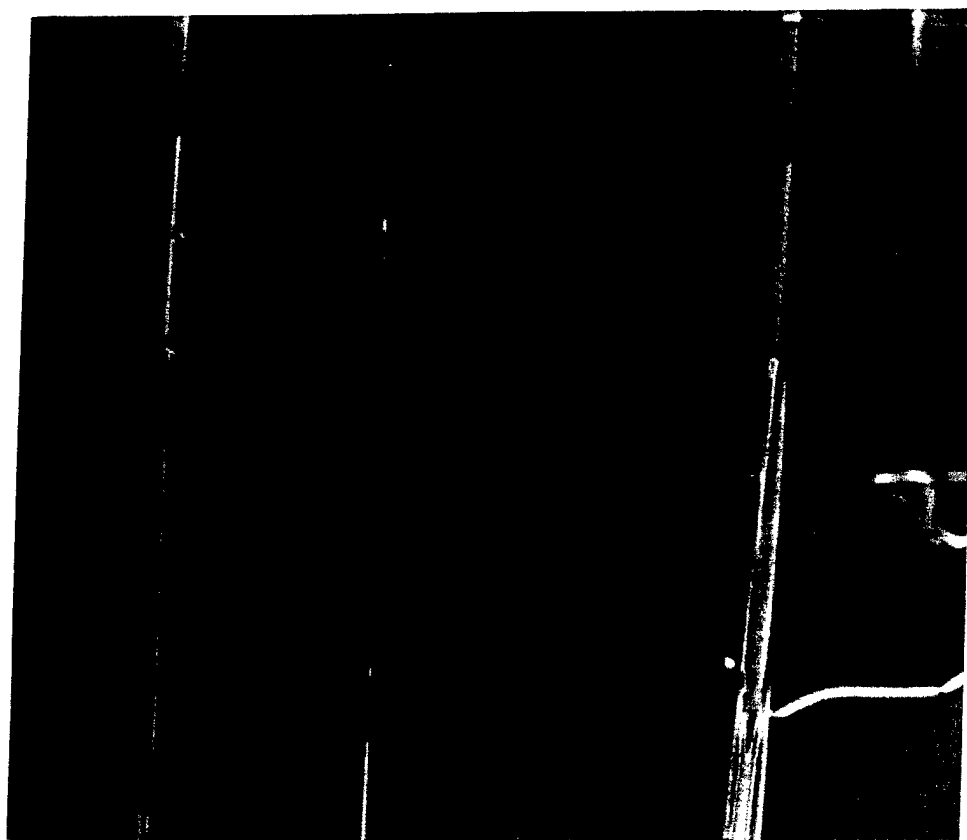


Figure A-3. Radiograph of Shot 16: Smooth Copper Wire.

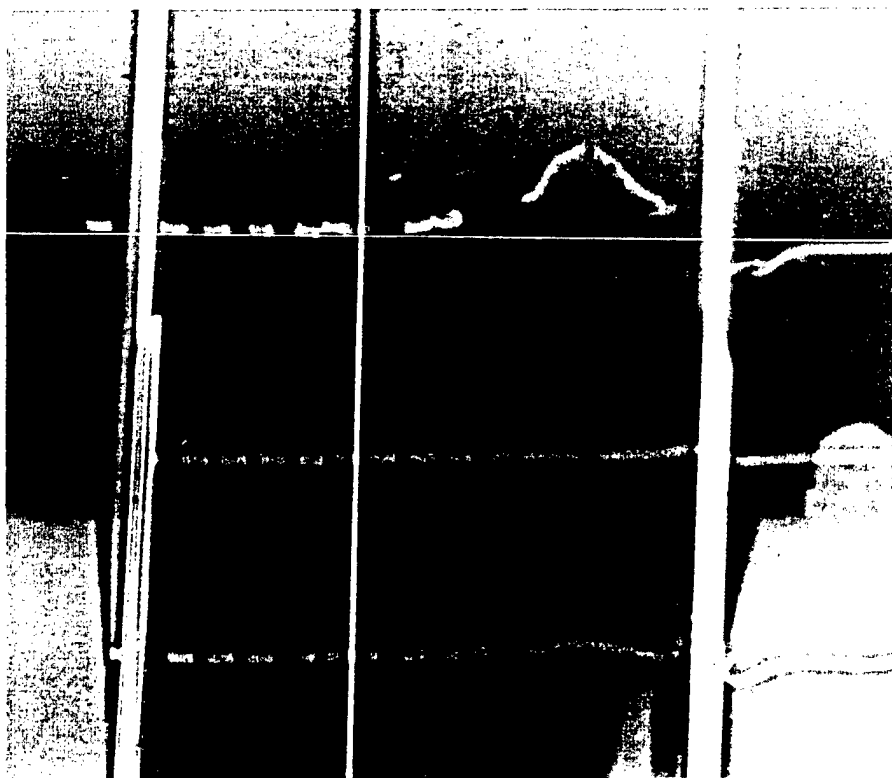


Figure A-4. Radiograph of Shot 17: Segmented Copper Wire.

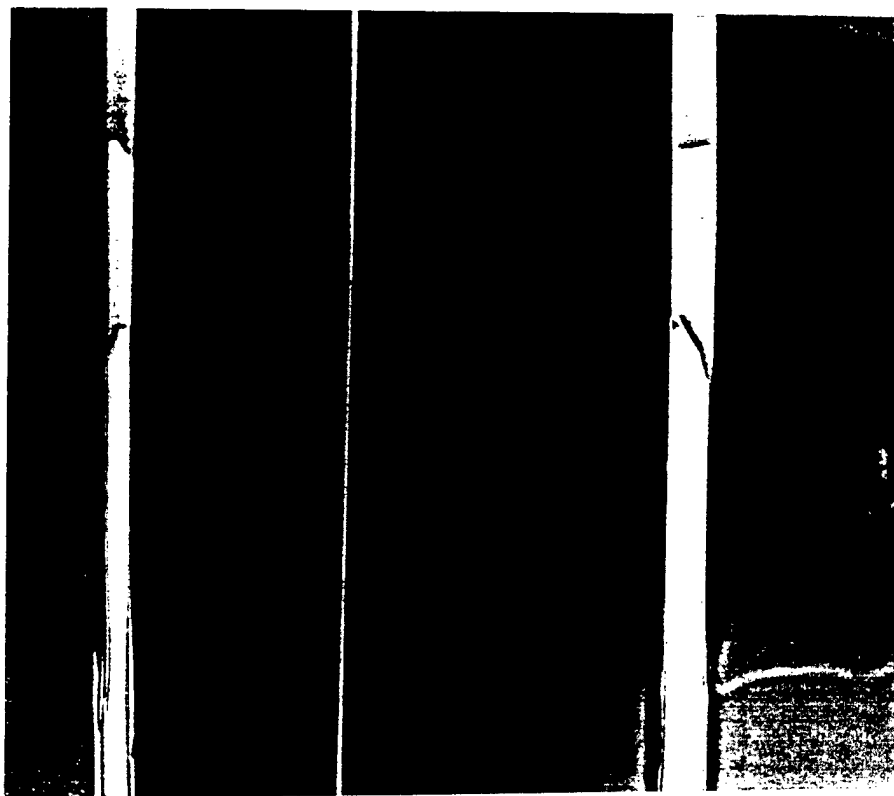


Figure A-5. Radiograph of Shot 18: Smooth Aluminum Wire.



Figure A-6. Radiograph of Shot 19: Segmented Aluminum Wire.

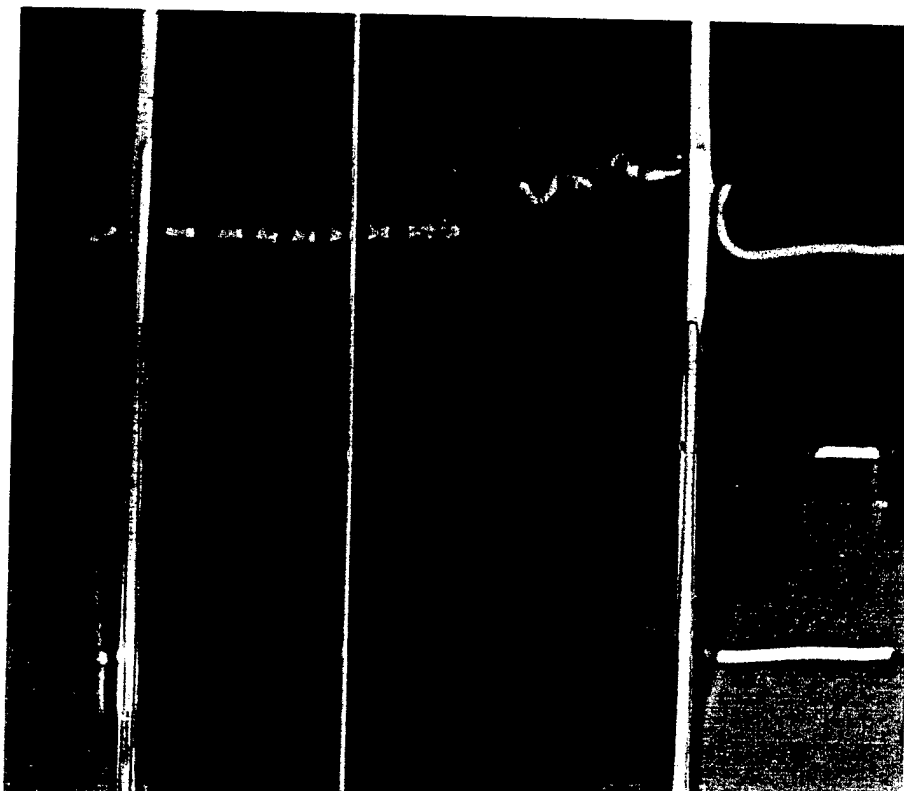


Figure A-7. Radiograph of Shot 20: Segmented Copper Wire.

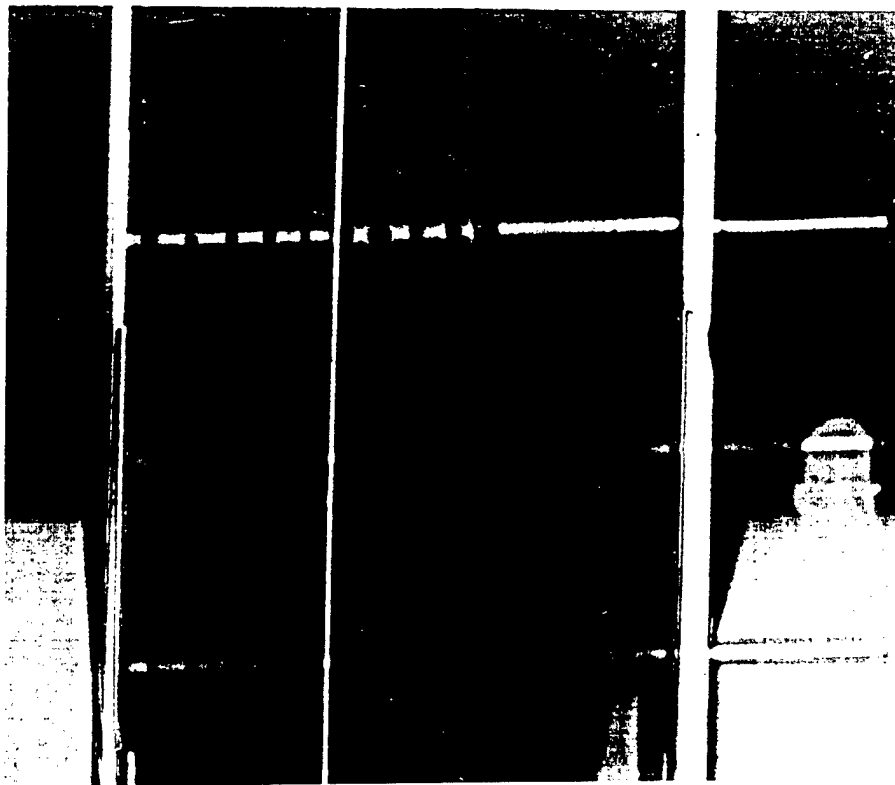


Figure A-8. Radiograph of Shot 21: Segmented Stainless Steel Wire.

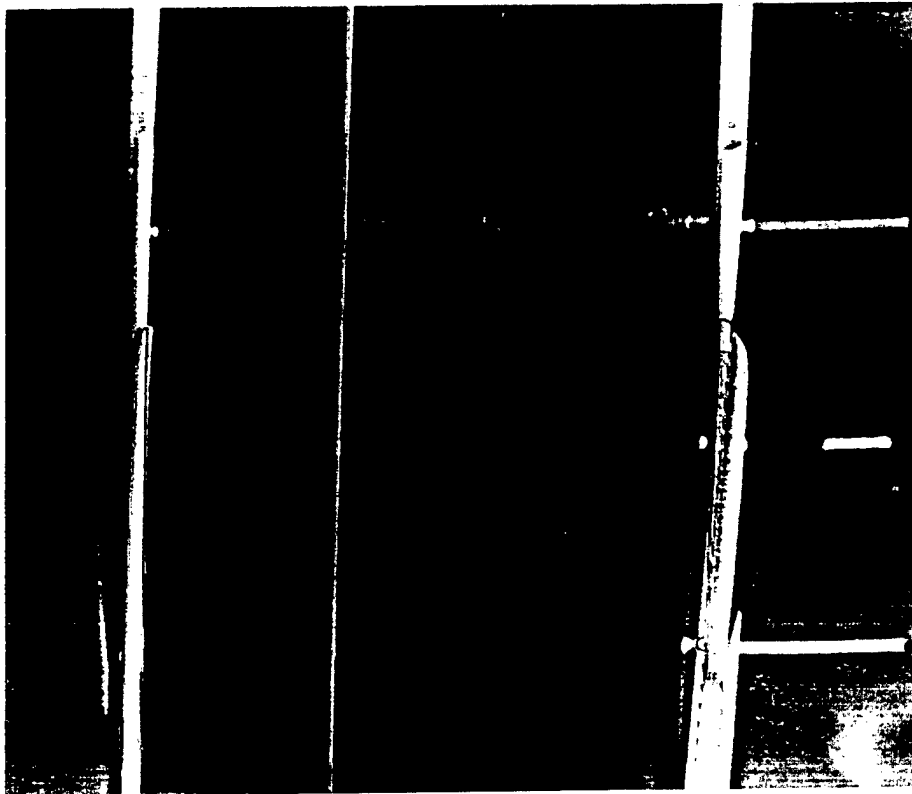


Figure A-9. Radiograph of Shot 22: Smooth Stainless Steel Wire.



Figure A-10. Radiograph of Shot 23: Sawtooth Brass Wire.

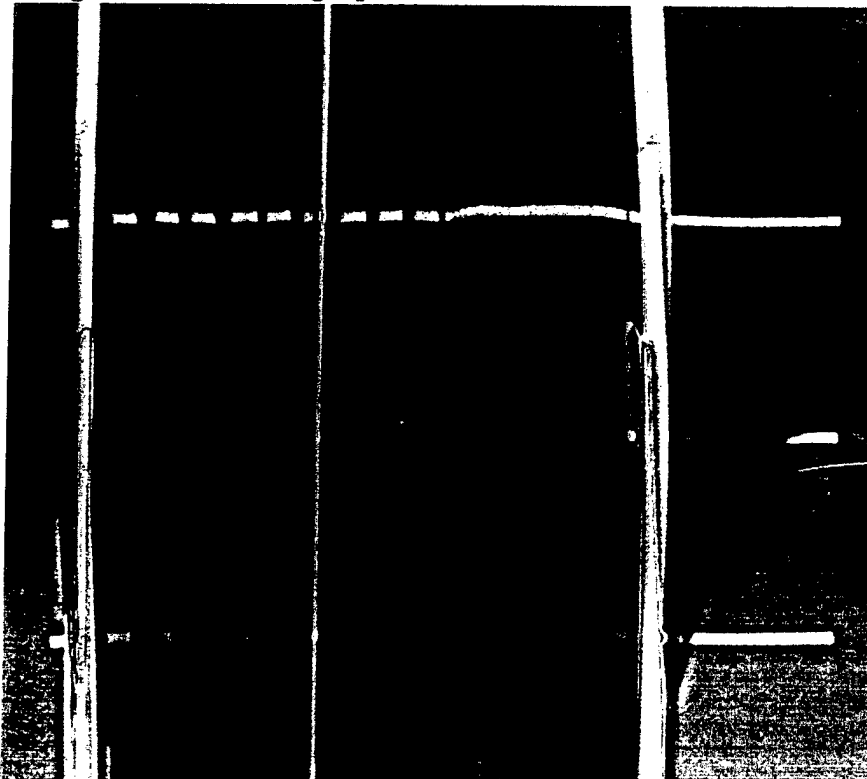


Figure A-11. Radiograph of Shot 24: Segmented Brass Wire.

INTENTIONALLY LEFT BLANK

REFERENCES

- A-1. Fischer, M.L., Pollock, C.E., and Butz, D.J., "Study of Electromagnetic Armor and Its Effect on Shaped Charge Jets," Battelle Columbus Operations Report R-6290, 28 February 1992.
- A-2. Filbey, G.L., Private Communication, 1996.
- A-3. Babkin, A.V., Kruzhkov, V.A., Ladov, S.V., Marinin, V.M., and Federov, S.V., "The Behavior of Metallic Shaped Charge Jets under the Action of a Current Pulse," *Proc. 7th International Conference on the Generation of Megagauss Magnetic Fields and Related Topics*, Nova Science Publishers, Inc., Albuquerque NM, November 1992, p.309.
- A-4. Filbey, G.L., Bruchey, W.J., Dehn, J.T., Huang, Y.I., Keele, M.J., and Kleponis, D.S., "Viper and Dragon Shaped Charge Jets Perturbed by Large Axial Currents (U)," *Proceeding Third Ballistics Symposium on Classified Topics and Controlled Topics*, Laurel MD, November 14-15, 1995, pp. 15-22 (SECRET).
- A-5. Hummer, C.R., and Hollandsworth, C.E., "Experiments on the Interaction Between Shaped Charge Jets and Axial Electric Currents: Pulsed Power Source and Diagnostics (U)," U.S. Army Research Laboratory Report ARL-TR-1452, August 1997 (SECRET).
- A-6. Keele, M.J., Kleponis, D.S., Hummer, C.R., and Hollandsworth, C.E., "Experiments on the Interaction Between Shaped Charge Jets and Axial Electric Currents: Walker Plate Experiments (U)," U.S. Army Research Laboratory Report, in press (SECRET).

INTENTIONALLY LEFT BLANK

<u>NO. OF COPIES</u>	<u>ORGANIZATION</u>	<u>NO. OF COPIES</u>	<u>ORGANIZATION</u>
2	ADMINISTRATOR DEFENSE TECHNICAL INFO CENTER ATTN DTIC OCP 8725 JOHN J KINGMAN RD STE 0944 FT BELVOIR VA 22060-6218	1	COMMANDER USAARDEC ATTN AMSTA AR FSA T GORA PICATINNY ARSENAL NJ 07806-5000
1	DIRECTOR US ARMY RESEARCH LABORATORY ATTN AMSRL CS AL TA REC MGMT 2800 POWDER MILL RD ADELPHI MD 20783-1197	2	NCSU ATTN JG GILLIGAN M BOURHAM BOX 7909 1110 BURLINGTON ENGR LABS RALEIGH NC 27695-7909
1	DIRECTOR US ARMY RESEARCH LABORATORY ATTN AMSRL CI LL TECH LIB 2800 POWDER MILL RD ADELPHI MD 207830-1197	4	INST FOR ADVANCED TECHNOLOGY ATTN DR H FAIR DR I MCNAB P H SULLIVAN DR K T HSIEH 4030 2 W BRAKER LANE AUSTIN TX 78759-5329
1	DIRECTOR US ARMY RESEARCH LABORATORY ATTN AMSRL CS AL TP TECH PUB BR 2800 POWDER MILL RD ADELPHI MD 20783-1197	1	STATE UNIV OF NEW YORK ATTN DR W J SARGEANT DEPT OF ELEC ENGR BONNER HALL RM 312 BUFFALO NY 14260
1	DIRECTOR US ARMY RESEARCH LABORATORY ATTN AMSRL D DR J LYONS 2800 POWDER MILL RD ADELPHI MD 20783-1197	1	SAIC ATTN DR WOODWARD WAESCHE 1710 GOODRIDGE DR MCLEAN VA 22102
1	DIRECTOR US ARMY RESEARCH LABORATORY ATTN AMSRL DD J J ROCCHIO 2800 POWDER MILL RD ADELPHI MD 20783-1197	1	SCIENCE APPLN INTL CORP ATTN KEITH A JAMISON 1247-B N EGLIN PKWY SHALIMAR FL 32579
1	HQ DEFENSE SPEC WEAPONS AGENCY ATTN D LEWIS 6801 TELEGRAPH RD ALEXANDRIA VA 22310-3398	2	SCIENCE APPLICATIONS INC ATTN J BATTEH L THORNHILL 1225 JOHNSON FERRY RD SUITE 100 MARIETTA GA 30068
1	UNITED DEFENSE LP ARMAMENT SYSTEMS DIV ATTN R JOHNSON 4800 E RIVER RD MINNEAPOLIS MN 55421-1498	1	IAP RESEARCH INC ATTN JOHN P BARBER 2763 CULVER AVE DAYTON OH 45429-3723
2	US ARMY RESEARCH OFFICE ATTN DR DAVID M MANN DR ROBERT SHAW PO BOX 12211 4300 S MIAMI BLVD RSRCH TRIANGLE PK NC 27709-2211	2	CDR TARDEC ATTN AMSTA JS J THOMPSON AMSTA TR T FURMANIAK WARREN MI 48397-5000
		1	CDR TAAC ARMAMENTS CMD SURVIVABILITY TECH CENTER ATTN SFAE GCSS W GSI H J ROWE WARREN MI 43897-5000

NO. OF
COPIES ORGANIZATION

2 SAIC
ATTN A J TOEPFER
R PARKINSON
2109 AIR PARK RD
ALBUQUERQUE NM 87106

ABERDEEN PROVING GROUND

2 DIRECTOR
US ARMY RESEARCH LABORATORY
ATTN AMSRL CI LP (TECH LIB)
BLDG 305 APG AA

30 DIR ARL
ATTN AMSRL WM P E SCHMIDT
AMSRL WM PA W OBERLE
G WREN K WHITE
AMSRL WM PB A ZIELINSKI
AMSRL WM T W MORRISON
AMSRL WM TA W BRUCHEY
G FILBEY M KEELE (5 CYS)
D KLEPONIS W GILLICH
AMSRL WM TE A NIILER
P BERNING C HUMMER
C HOLLANDSWORTH (5 CYS)
L KECSKES T KOTTKE
J POWELL A PRAKASH
H SINGH C STUMPFEL
G THOMSON

REPORT DOCUMENTATION PAGE

Form Approved
OMB No. 0704-0188

Public reporting burden for this collection of information is estimated to average 1 hour per response, including the time for reviewing instructions, searching existing data sources, gathering and maintaining the data needed, and completing and reviewing the collection of information. Send comments regarding this burden estimate or any other aspect of this collection of information, including suggestions for reducing this burden, to Washington Headquarters Services, Directorate for Information Operations and Reports, 1215 Jefferson Davis Highway, Suite 1204, Arlington, VA 22202-4302, and to the Office of Management and Budget, Paperwork Reduction Project (0704-0188), Washington, DC 20503.

1. AGENCY USE ONLY (Leave blank)		2. REPORT DATE December 1998	3. REPORT TYPE AND DATES COVERED Final	
4. TITLE AND SUBTITLE Conduction in Electrically Exploded Wires of Nonuniform Diameters			5. FUNDING NUMBERS PR: 1L162618AH80	
6. AUTHOR(S) Hollandsworth, C.E., Powell, J.D., Keele, M.J., Hummer, C.R. (all of ARL)				
7. PERFORMING ORGANIZATION NAME(S) AND ADDRESS(ES) U.S. Army Research Laboratory Weapons & Materials Research Directorate Aberdeen Proving Ground, MD 21010-5066			8. PERFORMING ORGANIZATION REPORT NUMBER	
9. SPONSORING/MONITORING AGENCY NAME(S) AND ADDRESS(ES) U.S. Army Research Laboratory Weapons & Materials Research Directorate Aberdeen Proving Ground, MD 21010-5066			10. SPONSORING/MONITORING AGENCY REPORT NUMBER ARL-TR-1773	
11. SUPPLEMENTARY NOTES				
12a. DISTRIBUTION/AVAILABILITY STATEMENT Approved for public release; distribution is unlimited.			12b. DISTRIBUTION CODE	
13. ABSTRACT (Maximum 200 words) Recent work by Me-Bar and Harel, intended to characterize the conduction characteristics of exploding segmented wires, is extended. A set of experiments on conductors composed of various materials and in various geometries was undertaken. The experimental work is complemented by two-dimensional calculations in which the magnetic diffusion equation is solved for the problems at hand. Results from these calculations are used to explain the behavior observed in the experiments. It is also observed from the calculations that different results for segmented wires might be obtained if the plasma, resulting from partial explosion of the wires, is confined radially around the wire. A set of experiments to test this contention was undertaken and produced results in good qualitative agreement with the theoretical predictions. Physical reasons for the observed behavior, as well as possible methods for ameliorating undesired effects, are indicated.				
14. SUBJECT TERMS electrical conduction plasma arc exploding wire segmented wire			15. NUMBER OF PAGES 50	
			16. PRICE CODE	
17. SECURITY CLASSIFICATION OF REPORT Unclassified	18. SECURITY CLASSIFICATION OF THIS PAGE Unclassified	19. SECURITY CLASSIFICATION OF ABSTRACT Unclassified	20. LIMITATION OF ABSTRACT	